The Calculated Infrared Spectra of Functionalized Hexamethylenetetramine (HMT) Molecules

Partha P. Bera[1,2] , Scott A. Sandford[1] , Timothy J. Lee[3] , and Michel Nuevo[1,2]
[1] NASA Ames Research Center, MS 245-6, Moffett Field, CA 94035, USA
[2] Bay Area Environmental Research Institute, NASA Research Park, MS 18-4, Moffett Field, CA 94035, USA
[3] NASA Ames Research Center, MS 245-3, Moffett Field, CA 94035, USA; Timothy.J.Lee@nasa.gov

Abstract

Numerous laboratory studies have shown that exposure of mixed ices of astrophysical interest to ionizing radiation leads to the production of large numbers of new, more complex compounds. A significant portion of these new species appear to belong to a family of molecules that consist of hexamethylenetetramine (HMT; $C_6H_{12}N4$) and hexamethylenetetramine to which different functional side groups have been added. In this paper, we present the computed harmonic vibrational infrared spectra of a number of HMT variants that include HMT-OH, HMT-NH$_2$, HMT-CH$_3$, HMT-CN, HMT-OCN, HMT-OCH$_3$ HMT-CH(OH)CHO, and HMT-NHCHO. Since all of the members of this family share the common HMT framework as a major part of their structure, they produce a number of infrared bands that fall at similar positions and have similar strengths, which will make them easier to detect in space as a family. However, each molecular HMT variant also produces additional unique bands due to its attached side group, so it is possible to distinguish between different variants.

Key words: astrobiology – astrochemistry – ISM: molecules – methods: laboratory: molecular – methods: numerical – molecular processes

1. Introduction

Numerous previous laboratory simulation experiments have shown that mixed molecular ices of astrophysical interest undergo rich, solid-state chemistry when exposed to ionizing radiation in the form of UV photons or cosmic rays followed by subsequent warming of the ice. The irradiation produces numerous ions and radicals within the ices that recombine as the ice warms to form a wide variety of new, more complex molecular species (e.g., Allamandola et al. 1988; Bernstein et al. 1995; Moore & Hudson 1998; Gerakines et al. 2001; Dworkin et al. 2004; Meierhenrich et al. 2005; Bennett & Kaiser 2007; Callahan et al. 2013). Many of these species are of astrobiological interest and include amino acids (Bernstein et al. 2002a; Muñoz Caro et al. 2002; Nuevo et al. 2007, 2008), amphiphiles (Dworkin et al. 2001), sugars and related compounds (Nuevo et al. 2015, 2018; Meinert et al. 2016), quinones (Bernstein et al. 1999, 2001, 2002b, 2003; Ashbourn et al. 2007), nucleobases (Nuevo et al. 2009, 2012, 2014; Materese et al. 2013, 2017, 2018; Sandford et al. 2015), and a host of other organic compounds like ethers, urea, and hydantoin (Bernstein et al. 1999; Nuevo et al. 2010; de Marcellus et al. 2011). Mechanisms for the formation of nucleic acid bases in ices have been investigated using theoretical calculations (Bera et al. 2010, 2016, 2017).

Hexamethylenetetramine (also called methenamine, hexamine, aminoform, urotropin, and a host of other names, and hereafter are simply referred to as HMT; Figure 1(a)) was one of the first complex molecules uniquely identified in the organic residues recovered at room temperature after the irradiation of astrophysical ice analogs in the laboratory (Bernstein et al. 1995). While just one of a very large number of compounds formed when astrophysical ice analogs were exposed to ionizing radiation, it is one of the most abundant individual molecular products (Bernstein et al. 1995; Cottin et al. 2001). A recent isotopic substitution study (Materese

et al. 2019) demonstrated that HMT-methanol (HMT with a CH$_2$OH group substituting for a peripheral H atom) is also an abundant product, and a mass spectral study (Muñoz Caro & Schutte 2003) suggested that a number of HMT variants in which different chemical functional groups are attached to a central HMT cage are also made. This suggests that the complex organic residues produced when many astrophysical ices are processed by ionizing radiation may contain an abundant family of HMT variants.

HMT is of considerable astrobiological interest because its degradation products include amino acids (Hulett et al. 1971), a variety of N-heterocycles (Vinogradoff et al. 2018), and a host of other organics such as nitriles (Bernstein et al. 1994, 1995; Cottin et al. 2002). HMT variants in which one or more peripheral H atoms are substituted with some other chemical functional group would be expected to produce additional, but similar suites of compounds.

HMT is a highly symmetric molecule having tetrahedral (T_d) symmetry. However, singly substituted HMT molecules have much lower C_1 symmetry and, as a result, will generally produce spectra with larger numbers of infrared (IR) active bands. However, since these molecules all contain the same central HMT cage structure, many of the bands, including most of the stronger ones, will fall at very similar spectral positions. Since all of the members of the HMT "family" of molecules will produce many IR bands that overlap, it may potentially be easier to detect these molecules in space as a family. Also, since each molecular HMT variant also produces additional unique bands due to its attached side group, it should be possible, at least in principle, to distinguish between different variants if they are present.

Here, we report the computed IR spectra of HMT-OH, HMT-NH$_2$, HMT-CH$_3$, HMT-CN, HMT-OCN, HMT-OCH$_3$ HMT-CH(OH)CHO, and HMT-NHCHO using ab initio quantum chemistry methods, and compare them to Materese et al. (2019) results for HMT and HMT-methanol (HMT-CH$_2$OH).
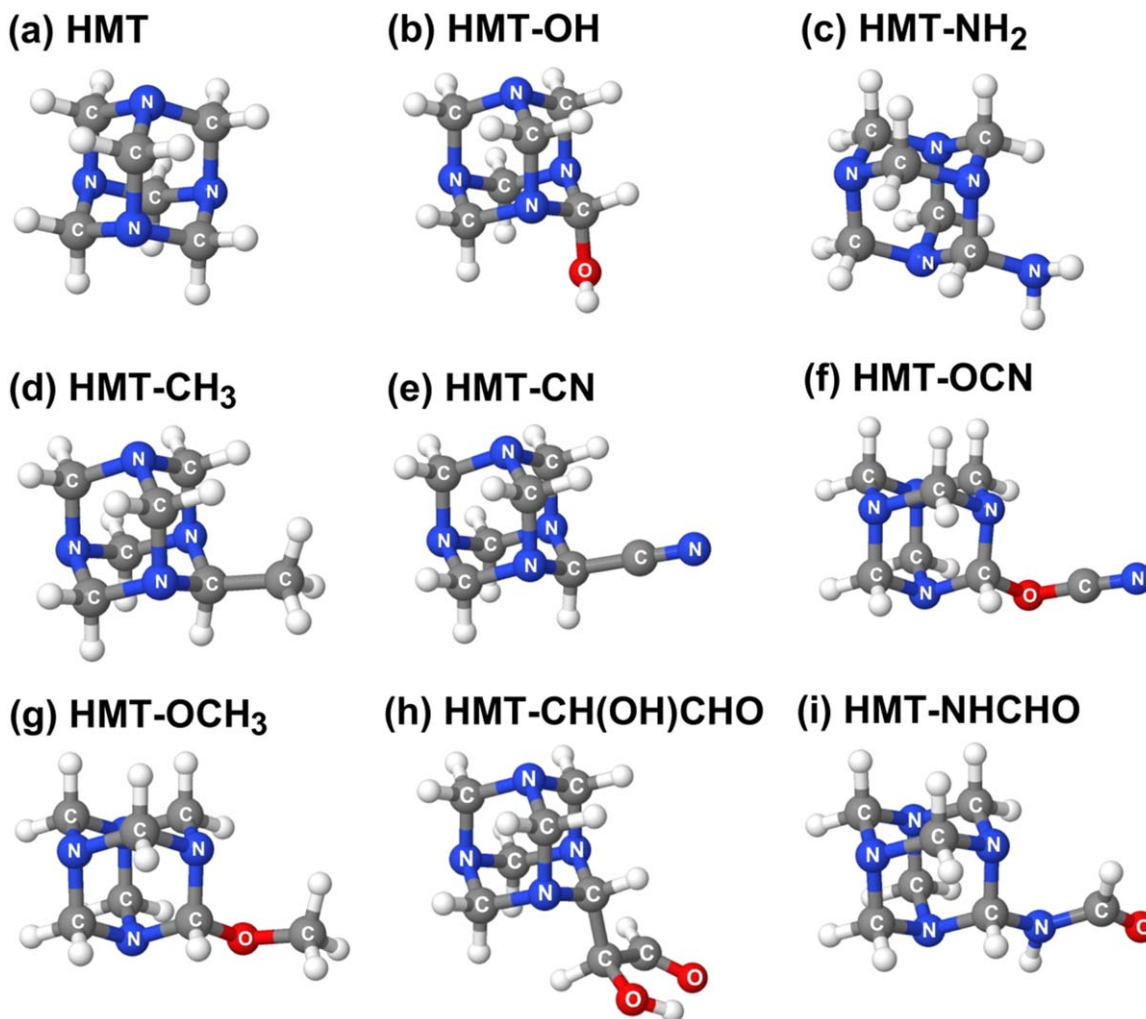
Figure 1. Structures computed for (a) hexamethylenetetramine (HMT), (b) HMT-OH, (c) HMT-NH$_2$, (d) HMT-CH$_3$, (e) HMT-CN, (f) HMT-OCN, (g) HMT-OCH$_3$, (h) HMT-CH(OH)CHO, and (i) HMT-NHCHO using the ωB97X-D/cc-pVTZ method.

The results reinforce the suggestion that this family of molecules may be detectable via some of the shared strong bands associated with the central HMT cage, and better defines how different individual variants might be identified.

Since all of these other HMT variants lack the high level of symmetry of HMT, they should produce rotational transitions that can be observed at longer wavelengths, although establishing the exact positions of these transitions is challenging.

2. Computational Procedures

Structural and spectroscopic characteristics of the HMT variants presented here have been investigated using density functional theory (DFT) using the ωB97X-D functional together with a correlation-consistent polarized triple-zeta (cc-pVTZ) basis set (Dunning 1989) that includes *spdf* functions for the C, N, and O atoms, and *spd* functions for H atoms. All calculations were performed with the Q-Chem 5 quantum chemistry program package (Shao et al. 2015). Structural parameters obtained using this level of theory are expected to be accurate to within $\sim 10^{-3}$ Å relative to experimental values. The ωB97X-D functional has been used because it has been shown to perform well across the board in predicting equilibrium geometries, vibrational IR spectra, as well as other molecular properties (Bera et al. 2013, 2015; Minenkov et al.

2012; Wang et al. 2015; Mardirossian & Head-Gordon 2017). In particular for vibrational IR spectra, see the comparisons presented in the Computational Chemistry Comparison and Benchmark DataBase project (Johnson 2018), where it is shown that ωB97X-D generally has a smaller range of errors relative to the popular B3LYP functional. The gas-phase optimized geometrical structures of HMT-OH, HMT-NH$_2$, HMT-CH$_3$, HMT-CN, HMT-OCN, HMT-OCH$_3$, HMT-CH (OH)CHO, and HMT-NHCHO are presented in Figure 1. As indicated, their harmonic vibrational frequencies and double harmonic infrared intensities were also calculated using the ωB97X-D/cc-pVTZ method.

3. Results

The functional side groups substitute for one of the hydrogen atoms attached to a carbon atom from the HMT cage structure and thus lower the tetrahedral symmetry of HMT. All of the new HMT variants considered here possess C_1 symmetry due to the presence of their unique side groups. This lowering of symmetry causes the equal C−N bond lengths of HMT to become all unique. The C−N bonds that are closest to the side groups are affected the most, and the distortion effect gradually diminishes along the cage structure as one moves away from the side group. The CH$_3$, CN, and CH(OH)CHO side groups

Table 1
Bond Lengths (Å) of HMT and HMT-CH$_2$OH (from Materese et al. 2019), and of HMT-OH, HMT-NH$_2$, HMT-CH$_3$, HMT-CN, HMT-OCN, HMT-OCH$_3$, HMT-CH(OH)CHO, and HMT-NHCHO from This Work

Molecule	Framework Bonds		Side-group Bonds					
	CH	CN	CC	CN	CO	OH	CH	NH
HMT	1.091	1.465						
HMT-CH$_2$OH	1.091–1.093	1.464–1.473	1.520		1.411	0.956	1.092, 1.093	
HMT-OH	1.090–1.097	1.461–1.472			1.392	0.959		
HMT-NH$_2$	1.091–1.098	1.464–1.471		1.441				1.010
HMT-CN	1.090–1.093	1.464–1.471	1.472	1.146				
HMT-CH$_3$	1.089–1.093	1.464–1.475	1.518				1.088	
HMT-CHOHCHO	1.089–1.093	1.462–1.470	1.515, 1.537		1.203, 1.392	0.966	1.098, 1.099	
HMT-NHCHO	1.089–1.095	1.463–1.473		1.362, 1.442	1.207		1.100	1.008
HMT-OCN	1.089–1.091	1.444–1.475		1.151	1.286, 1.444			
HMT-OCH$_3$	1.080–1.091	1.464–1.472			1.386, 1.409		1.087–1.096	

Note. For common bonds such as CH and CN that appear many times in the HMT framework, only a range of bond lengths is given.

affect the C−N bond lengths the least. The C−C bond lengths in HMT-CH$_3$ and HMT-CHOHCHO are slightly shorter than the C−C single bond length in ethane. The C−C bond length in HMT-CN is even shorter due mainly to the sp^2 hybridization of the carbon atom in the C−N side group. Both the NH$_2$ and NHCHO side groups slightly shorten the C−N single bonds with the carbon atom in HMT, and also slightly alter the C–N single bonds in the HMT cage. The OH and OCH$_3$ side groups make rather short O−C single bonds between the O of the side group and the C of HMT, with lengths of 1.392 and 1.386 Å for OH and OCH$_3$, respectively. The O–C bond in HMT-OCN is comparatively longer at 1.444 Å. The presence of oxygen in the side groups OH, OCH$_3$, and OCN alters the C−N single bonds that are adjacent to the side groups inside the HMT cage structure rather dramatically. This effect is diminished farther away from the side group. All of these alterations in the C−N bond lengths in the cage structure are reflected in the vibrational frequencies. Table 1 provides a summary of the bond lengths associated with the molecules discussed here.

The computed IR band positions and intensities of the harmonic vibrational frequencies for HMT-OH, HMT-NH$_2$, HMT-CH$_3$, HMT-CN, HMT-OCN, HMT-OCH$_3$ HMT-CH(OH)CHO, and HMT-NHCHO are given in Tables 3 through 10, respectively (Appendix A). The corresponding spectra are presented graphically in Figure 2. Similar tables and figures for HMT and HMT-CH$_2$OH can be found in Materese et al. (2019).

The only IR active vibrational bands for HMT, some of which have very large intensities, are triply degenerate. Hence, the vibrational modes associated with the HMT framework vibrations are split into a number of weaker vibrational bands that include C–N and C–H stretching, HCH bending, and a number of torsional modes, due to the lowering of symmetry after the side-group substitution. For example, two sets of triply degenerate C–H stretching vibrations appear with large intensities: one set at 3058 cm^{-1}, each with an intensity of 106 km mol^{-1} (for a total IR intensity of 318 km mol^{-1}), and another set at 3111 cm^{-1}, each with an intensity of ~55 km mol^{-1} (for a total IR intensity of 164 km mol^{-1}). Side-group substitution can be seen as a perturbation on the overall HMT vibrational spectrum. Thus, one might expect that the vibrational modes that are IR inactive in the spectrum of HMT are IR active with small IR intensities in the spectra of the substituted HMT molecules, resulting in a large number of bands with very small IR intensities compared with the most intense modes. However, for the C–H stretches, this is not the case, in general. There are usually one or two C–H stretches with very small IR intensities, but the intensity seen in HMT is mostly spread out across the rest of the C–H stretches in the HMT molecules with a side group. For the other HMT vibrational bands that exhibit large IR intensities, it is possible to correlate some of these bands with the large-intensity vibrational bands in the substituted HMTs, as we found for HMT-CH$_2$OH. Specifically, HMT has two triply degenerate bands with large IR intensities at 1299 cm^{-1} (210 km mol^{-1}) and 1063 cm^{-1} (438 km mol^{-1}). Examination of Tables 3–10 shows that indeed there are three vibrational bands near these values that possess large IR intensities, and sometimes there is a fourth band nearby that also has a large IR intensity, suggesting that this was an IR inactive band in HMT that has borrowed some of the IR intensity through coupling.

Among all of the substituted HMT molecules studied in the present work, both HMT-OH (Table 3) and HMT-CH(OH)CHO (Table 9) produce a strong O–H stretching feature that falls at 3888 cm^{-1} and 3762 cm^{-1}, respectively. Both of these are shifted to lower frequencies compared with the 3925 cm^{-1} O–H band stretching band produced by HMT-CH$_2$OH (Materese et al. 2019).

There are two types of CO stretching bands that appear in the spectra of HMT substituted with side groups containing oxygen atoms: (i) C–O single bonds resulting from the attachment of the side groups to the HMT cage, and (ii) C=O double bonds that are conventional terminal carbonyl groups and that are found in the side groups alone. The strong C–O stretching frequency for the bond from the HMT cage and the oxygen from the OH group in HMT-OH (Table 3) appears at 1175 cm^{-1}. The other molecules in which such C–O stretching bands appear are HMT-OCN (1024 cm^{-1}, Table 7) and HMT-OCH$_3$ (1272 cm^{-1}, Table 8), and these also display large IR intensities. HMT-CH(OH)CHO (Table 9) and HMT-NHCHO (Table 7) display strong C=O features, at 1831 cm^{-1} and 1822 cm^{-1} respectively, assigned to the terminal aldehyde (CHO) moiety in the side group. The C–O stretching frequencies associated with the stretching mode of the O–C bond within the side groups in HMT-OCN (Table 7) and HMT-OCH$_3$ (Table 8) are 1079 cm^{-1} and 1187 cm^{-1}, respectively.
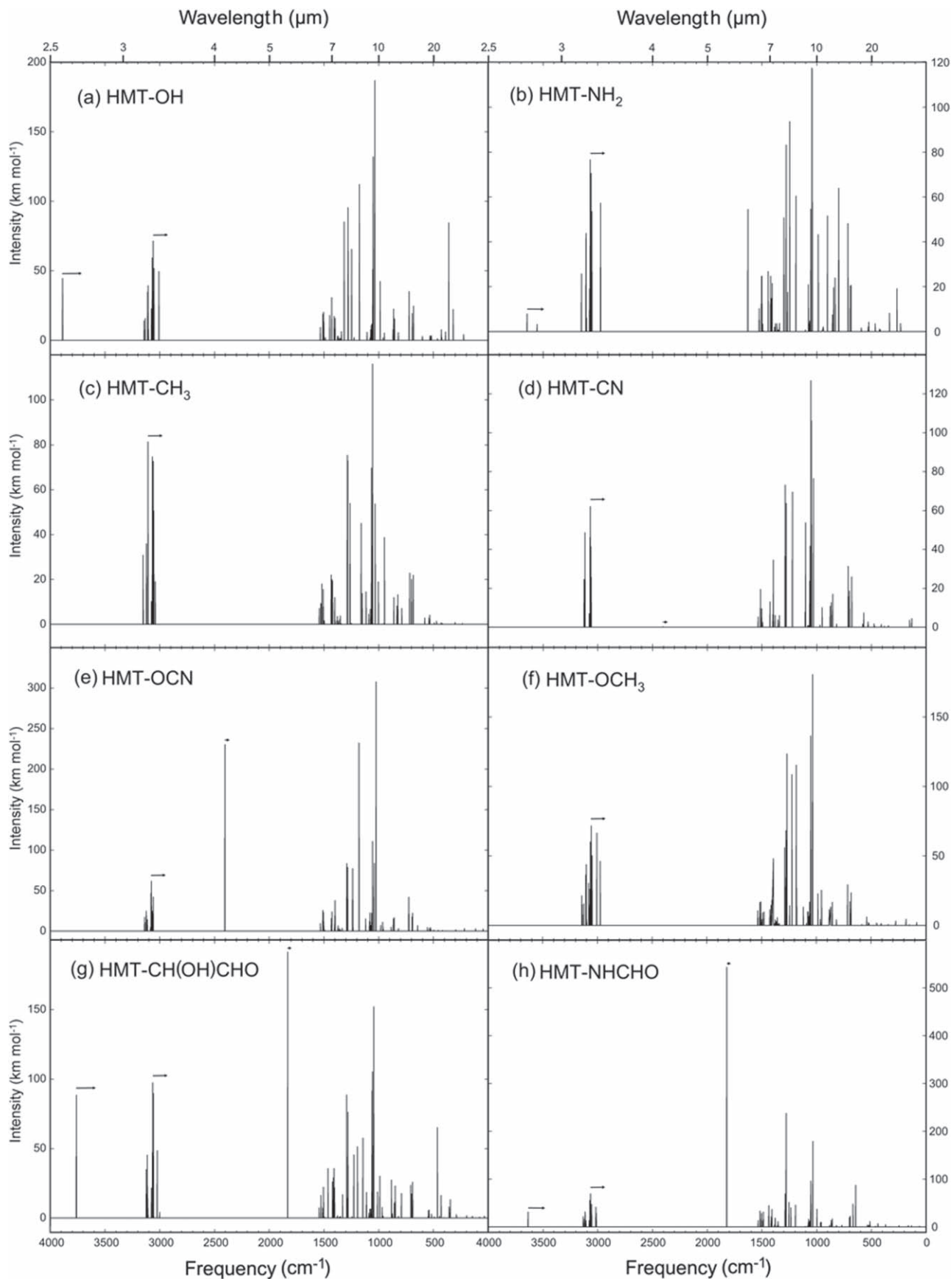
Figure 2. Computed harmonic vibrational spectra of (a) HMT-OH, (b) HMT-NH$_2$, (c) HMT-CH$_3$, (d) HMT-CN, (e) HMT-OCN, (f) HMT-OCH$_3$, (g) HMT-CH(OH)CHO, and (h) HMT-NHCHO. Arrows above the representative IR bands indicate the direction and magnitude of band shifts expected if anharmonicity were taken into account. C–C and C–N modes below 1600 cm^{-1} are expected to have anharmonic corrections of less than 25 cm^{-1}.

Similar to the case for O-containing side groups, there are two types of CN stretching bands that appear in the spectra of HMT substituted with side groups containing nitrogen atoms: (i) C−N single bonds resulting from the attachment of the side groups to the HMT cage, and (ii) C≡N triple bonds that are conventional terminal nitrile groups. The frequencies for the C−N stretching modes in HMT-NH$_2$ and HMT-NHCHO are 1190 and 1194 cm^{-1}, respectively. As indicated previously, the harmonic vibrational frequency of the terminal C≡N bond of HMT-OCN produces a very strong feature at 2405 cm^{-1} (see Figure 2(e)). Based on the anharmonicity corrections discussed below, the vibrational anharmonicity correction of this fundamental frequency is expected to shift to the red and fall closer to ~2360 cm^{-1}.

The values reported in Tables 3–10 will shift if anharmonicity is taken into account, with the magnitude of the shifts depending on the nature of the vibrational mode. For example, the average anharmonic correction for the C–H stretching modes in methane is approximately 137 cm^{-1} (Lee et al. 1995b), and this value corresponds to the largest anharmonic correction expected for any of the modes in HMT. Shifts of similar magnitudes would be expected for the C–H bands associated with the side groups in HMT-CH$_3$, HMT-CH(OH) CHO, HMT-NHCHO, and HMT-OCH$_3$. The O–H stretch in HMT-CH$_2$OH and HMT-OH will have a slightly larger anharmonic correction as evidenced by the average anharmonic correction for the frequencies of the O–H stretches in water of approximately 187 cm^{-1} (Huang & Lee 2008). Similarly, the N–H stretches in HMT-NH$_2$ and HMT-NHCHO will have a large anharmonic correction, probably similar to the ~164 cm^{-1} average value for the NH$_3$ molecule (Martin et al. 1992). From our experience, the anharmonic corrections for most of the other modes will be much smaller, i.e., less than 25 cm^{-1}, with the exception of the C≡N triple bonds that occur in the -CN and -OCN side groups, and the C=O double bonds that occur in the -CH(OH)CHO and -NHCHO side groups.

We can estimate the anharmonic correction for the C≡N triple bonds by examining the anharmonic corrections for the C≡N triple bond in the HCN (Lee et al. 1993), FCN, and ClCN molecules (Lee et al. 1995a). For HCN, the C≡N bond has an anharmonic correction of ~30 cm^{-1}, while the anharmonic corrections for the C≡N bond in FCN and ClCN are ~38 and ~33 cm^{-1}, respectively. Interestingly, the anharmonic correction increases as the atom bonded to the C atom becomes more electronegative, going from 30, to 33, to 38 cm^{-1} for HCN, ClCN, and FCN, respectively. A related observation is that the C≡N fundamental vibrational frequency for this series of molecules goes from 2097 (HCN), to 2216 (ClCN), to 2319 cm^{-1} (FCN). Therefore, as the moiety bonded to the C atom becomes more electron-withdrawing, the C≡N triple bond fundamental vibrational frequency increases significantly. Examining Tables 6 and 7, it is clear that the C≡N harmonic frequencies for HMT-CN and HMT-OCN are 2404 and 2405 cm^{-1}, respectively, suggesting that the HMT moiety itself is strongly electron-withdrawing. Thus, the vibrational anharmonicity correction of this fundamental frequency is expected to shift to the red by ~45 cm^{-1}. However, one significant difference between HMT-CN and HMT-OCN is that the IR intensity for the C≡N vibrational frequency is much larger for HMT-OCN (230 km mol^{-1}) relative to HMT-CN (0.3 km mol^{-1}).

In order to estimate the anharmonic correction for the C=O double bond in the -CH(OH)CHO and the -NHCHO side groups, we note that the anharmonic correction for the C=O double bond in formaldehyde (H$_2$CO) is ~31 cm^{-1} (Martin et al. 1993). As shown in Tables 9 and 10 and in Figure 2, the C=O double bond vibrational frequency in both HMT-CH (OH)CHO and HMT-NHCHO, which occurs near 1800 cm^{-1}, has a large IR intensity, with the latter value being very large at 543 km mol^{-1}.

Based on extensive experience in computing anharmonic vibrational IR frequencies (Fortenberry & Lee 2019), the estimated anharmonic corrections given above should be accurate to within about ±10 cm^{-1} since specific stretching vibrations will exhibit a characteristic frequency. There is one caveat, though, as larger molecules tend to have more Fermi and other types of resonances, which will complicate the vibrational IR spectrum by adding more vibrational bands and sharing IR intensity between the various bands (see, e.g., Mackie et al. 2015). This will be especially true for the C–H, N–H, and O–H stretching regions because combinations or overtones of many skeletal vibrational modes will approximately equal the C–H, N–H, or O–H fundamental vibrational frequencies. Furthermore, it is becoming possible to compute the anharmonic corrections for larger molecules, which has shown that typical anharmonic corrections for stretching vibrations remain consistent with those from smaller molecules (Boese & Martin 2004; Cané et al. 2007; Barone et al. 2014; Mackie et al. 2018). However, such calculations are expensive and are beyond the scope of the present study.

4. Discussion and Implications

4.1. The Search for HMT and Other HMT Variants in Space

4.1.1. Vibrational Modes of HMT and Its Variants in the Infrared

The high symmetry of HMT results in it having a relatively simple IR spectrum for a molecule of its size. Indeed, a significant number of its vibrational modes are degenerate and only the T_2 triply degenerate modes are IR active (Materese et al. 2019). The addition of any side group to HMT breaks this symmetry. This results in a more complex spectrum, because (i) the lower symmetry splits degenerate bands, (ii) the side group breaks the symmetry of the HMT cage, causing some IR inactive modes to become weakly active, and (iii) the side group produces new bands of its own. This increased spectral complexity is apparent for all of the HMT variants shown in Figure 2.

It is clear, however, that while the addition of a side group changes the spectrum of the original HMT considerably, it does not greatly affect some of the stronger bands in the spectrum of pure HMT. In particular, the strongest bands produced by HMT near 1267 and 1045 cm^{-1} (7.895 and 9.566 μm, respectively), both associated with antisymmetric C–N stretching modes, do not change greatly in position or relative strengths in the spectrum of the other variants. This is also true of a number of bands of more moderate intensity that are associated with cage vibrations, including the HMT-OH modes at 1277 and 1279 cm^{-1}. These similarities are largely due to vibrations that are all associated with the main cage structure of the HMT skeleton, which is similar for HMT and all of its variants.

This spectral behavior offers a potential opportunity to search for the HMT family of molecules in space. Previous and recent laboratory work (Bernstein et al. 1995; Muñoz Caro & Schutte 2003; Muñoz Caro et al. 2004; Materese et al. 2019)

indicates that HMT and its variants are some of the most abundant products formed when mixed molecular ices of astrophysical relevance are irradiated. Laboratory experiments suggest that the column densities of HMT alone can be expected to be slightly more than 1% of the original ice's total column density (Bernstein et al. 1995; Materese et al. 2019), and the simultaneous production of other HMT variants will only add to this abundance. Thus, given that the strongest HMT-related IR bands have high intrinsic intensities and provide good spectral contrast (the lines are typically $\sim$15–30 cm^{-1} wide in the solid state), they may well be detectable as weak IR absorption bands in the right environments.

The most likely environments in which HMT and its variants might be detected would be those in which astrophysical ices that have been exposed to ionizing radiation are being sublimed or sputtered away. Under these conditions, HMT and its variants will be produced as the ice dissipates and will reside either in organic residues on the surfaces of grains or be released into the gas phase. Environments that could provide these conditions would include the clouds in star-forming regions and surrounding protostellar objects, disks of proto-planetary systems, and perhaps on Saturn's moon Titan.

Since the structural nature of HMT and its variants results in some of these molecules' strongest IR bands falling at nearly the same spectral positions, the overall absorption in these bands will be stronger than those produced by any single variant. Figure 3 shows a plot in which all of our calculated spectra are superimposed, and it demonstrates how many of the stronger features of these molecules coadd. It may therefore be possible to detect the overall family of HMT-related compounds by searching for the family's characteristic bands, particularly the two strong bands near 1267 cm^{-1} (7.893 μm) and 1045 cm^{-1} (9.569 μm). Should these stronger bands be detected in the correct relative proportions together with some of the weaker bands, this would be strong evidence supporting the presence of this family of molecules in space. Indeed, Figure 4 in Bernstein et al. (1995) shows that HMT is readily identified via its vibrational IR frequencies and that spectral confusion does not hide HMT even though there are potentially hundreds or thousands of new compounds produced in their experiments. Establishing which individual members of the overall family are present would be a more difficult challenge as it would require the detection of (usually) weaker bands specific to the side groups of individual family members.

4.1.2. Rotational Transitions at Longer Wavelengths

HMT is a spherical top molecule whose high degree of symmetry results in the molecule having no dipole moment, so it is not expected to produce observable rotational bands at longer wavelengths. However, the addition of side groups to HMT breaks the symmetry and results in asymmetric top molecules that have nonzero dipole moments whose values depend on the nature of the side group. Table 2 contains the computed rotational constants and dipole moments for HMT and HMT-CH$_2$OH from Materese et al. (2019) as well as all the HMT variants studied in the present work.

All of these HMT variants would be expected to produce detectable rotational lines that fall in the submillimeter to millimeter spectral range. Given the spectral confusion
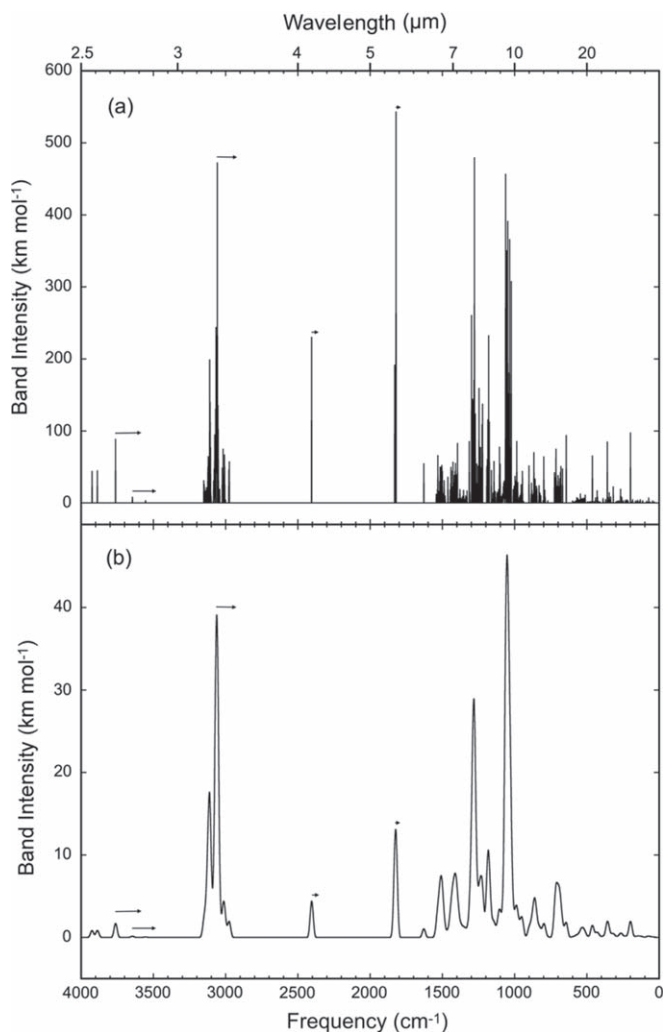
Figure 3. Composite spectra consisting of the coaddition of the computed spectra of HMT-OH, HMT-NH$_2$, HMT-CH$_3$, HMT-CN, HMT-OCN, HMT-OCH$_3$, HMT-CH(OH)CHO, and HMT-NHCHO, and the computed spectra of HMT and HMT-CH$_2$OH from Materese et al. (2019). Individual spectra of HMT and HMT-CH$_2$OH can be found in Materese et al. (2019), while the spectra of all other HMT-related species are from the present work (see Figure 2). The bands in panel (a) have been plotted with a width of 1 cm^{-1} so the spectrum is roughly equivalent to what would be expected if the molecules were in the gas phase. In panel (b), the bands have all been smoothed to have an FWHM of 25 cm^{-1} to better represent how these features would look if the molecules were in the solid state in grain mantles. Arrows above the representative IR bands indicate the direction and magnitude of band shifts expected if anharmonicity were taken into account. C–C and C–N modes below 1600 cm^{-1} are expected to have anharmonic corrections of less than 25 cm^{-1}.

expected for the infrared vibrational modes of HMT and its variants, rotational transitions could potentially offer the best hope for identifying individual HMT variants. Unfortunately, calculating the exact positions of these rotational lines will be difficult due to the relatively large size of these molecules; rotational line predictions typically need to be accurate to 1 MHz to assign individual molecules. Such calculations require a full consideration of anharmonic effects, which is very difficult and computationally very expensive. Nevertheless, these computational results should provide initial guidance as to where to search for these lines in a future laboratory experiment.

Table 2
Rotational Constants (A, B, and C, in cm^{-1} and GHz) and Dipole Moments (Debye) for HMT, HMT-CH$_2$OH, HMT-OH, HMT-NH$_2$, HMT-CH$_3$, HMT-CN, HMT-OCN, HMT-OCH$_3$, HMT-CH(OH)CHO, and HMT-NHCHO Calculated at the the ωB97X-D/cc-pVTZ Level of Theory

Molecule	A in cm^{-1} (GHz)	B in cm^{-1} (GHz)	C in cm^{-1} (GHz)	Dipole moment (D)
HMT[a]	0.06290 (1.88562)	…	…	0
HMT-CH$_2$OH[a]	0.06026 (1.80647)	0.02896 (0.86828)	0.02858 (0.85677)	1.42
HMT-OH	0.06278 (1.88220)	0.04432 (1.32860)	0.04422 (1.32566)	1.51
HMT-NH$_2$	0.06256 (1.87543)	0.04404 (1.32019)	0.04401 (1.31943)	1.23
HMT-CH$_3$	0.06228 (1.86714)	0.04318 (1.29454)	0.04316 (1.29395)	0.21
HMT-CN	0.06254 (1.87496)	0.03193 (0.957243)	0.03182 (0.953806)	4.27
HMT-OCN	0.59690 (1.78954)	0.02334 (0.699728)	0.02295 (0.688103)	5.46
HMT-OCH$_3$	0.06081 (1.82299)	0.03080 (0.923490)	0.03049 (0.913989)	1.24
HMT-CH(OH)CHO	0.05031 (1.50817)	0.01827 (0.547838)	0.01725 (0.517106)	3.06
HMT-NHCHO	0.06047 (1.81292)	0.02092 (0.627023)	0.02074 (0.621789)	4.54

Note.
[a] Values from Materese et al. (2019).

4.2. Astrophysical and Astrobiological Implications

HMT is known to produce a multitude of organics under the processes of photodegradation (Bernstein et al. 1994, 1995; Cottin et al. 2002), thermodegradation (Iwakami et al. 1968), hydrothermal degradation (Vinogradoff et al. 2018), and acidic hydrolysis (Hulett et al. 1971). Many of these products (e.g., amino acids and some N-heterocycles) are of astrobiological interest.

The degradation products of other HMT variants, including the ones discussed here are not currently known. However, it is likely that degradation processes acting on variants of HMT will produce similar products to those from HMT, i.e., methylamines, methane, ammonia, oxides of carbon and nitrogen, N-heterocycles, and a wider range of amino acids, plus additional products unique to the composition of their side groups. Degradation of HMT-related compounds in objects like asteroids could then potentially account for some of the wide variety of amino acids (more than 70; Shock & Schulte 1990; Sephton 2002) and other organic compounds observed in meteorites. Similar degradation of HMT and its derivatives may also take place on the surface of a planet, particularly those that support a hydrosphere.

Therefore, HMT, its variants, and their degradation products may play a significant role in prebiotic chemistry as precursors of a wide variety of compounds of biological significance. These compounds may have been part of the inventory available to play a role in the emergence of life on Earth, and since these molecules are made under conditions associated with star formation, they would be expected to play similar roles in other newly formed planetary systems.

5. Conclusions

Laboratory experiments suggest that a family of variants of hexamethylenetetramine (HMT) that consist of species having different side groups attached to the HMT cage is likely to be a common category of products resulting from the radiation processing of astrophysical ices. The computed IR spectra for members of this family show many similarities since many of the bands are associated with vibrations of the HMT cage that all of these molecules have in common. As a result, many of the IR bands of these HMT variants overlap, and these bands may offer a means of detecting this family of compounds in space. In contrast, the IR spectrum of each molecular variant also contains some unique bands associated with their particular side groups. The features associated with these side groups allow, in principle, a means of distinguishing different members of the HMT family from each other, although many of these features will be weaker since they do not overlap with the bands of other family members and could overlap with bands from other molecules that bear the same side groups. The main exception to this is a feature associated with the OCN side group at 2405 cm^{-1}, which has a very strong intrinsic strength.

Unlike HMT, which is highly symmetric, all of the HMT variants considered here have low (C_1) symmetry and therefore should produce rotational transitions that could be observed at longer wavelengths; although, establishing the exact positions of these transitions is challenging because it will be computationally very expensive.

Appendix A
Band Positions and Strengths for the HMT Variants Discussed in This Paper

Band positions and strengths for the HMT variants, HMT-OH, HMT-NH$_2$, HMT-CH$_3$, HMT-CN, HMT-OCN, HMT-OCH$_3$, HMT-CH(OH)CHO, and HMT-NHCHO, are presented in Tables 3–10, respectively.

Table 3
Harmonic Vibrational Frequencies (cm^{-1}) and IR Intensities (km mol^{-1}) of HMT-OH (C_1 Symmetry) Computed Using the ωB97X-D/cc-pVTZ Method

Frequency (cm^{-1})	Band Position (μm)	Intensity (km mol^{-1})	Frequency (cm^{-1})	Band Position (μm)	Intensity (km mol^{-1})
223	44.76	4.1	1277	7.829	64.2
318	31.49	22.2	1279	7.817	95.5
359	27.83	84.5	1314	7.608	85.2
389	25.72	6.0	1339	7.470	4.2
423	23.62	2.0	1340	7.463	6.3
427	23.43	7.6	1347	7.423	1.3
462	21.65	1.1	1355	7.379	1.4
517	19.33	3.3	1364	7.331	0.7
522	19.15	2.9	1370	7.299	2.9
531	18.84	3.2	1376	7.266	2.8
600	16.67	2.7	1398	7.153	15.8
680	14.70	24.6	1407	7.109	17.2
693	14.43	19.3	1428	7.003	30.7
722	13.85	35.1	1447	6.912	17.9
820	12.20	5.6	1487	6.724	1.9
854	11.72	15.4	1500	6.668	13.2
863	11.59	22.5	1503	6.653	20.2
868	11.52	7.6	1510	6.622	18.8
947	10.56	5.2	1532	6.526	9.3
961	10.40	1.8	3007	3.325	49.5
986	10.15	42.3	3052	3.276	51.8
1035	9.660	186.9	3055	3.274	35.0
1049	9.533	132.1	3061	3.267	71.5
1054	9.486	51.0	3069	3.258	59.3
1062	9.417	11.7	3076	3.251	22.6
1067	9.369	10.7	3103	3.223	7.7
1073	9.322	7.7	3107	3.219	39.3
1078	9.276	1.8	3111	3.215	34.7
1105	9.050	5.8	3132	3.193	15.7
1175	8.508	112.2	3144	3.180	14.0
1225	8.162	2.0	3888	2.572	44.5
1247	8.019	65.5	...	...	...

Table 4
Harmonic Vibrational Frequencies (cm^{-1}) and IR Intensities (km mol^{-1}) of HMT-NH$_2$ (C_1 Symmetry) Computed Using the ωB97X-D/cc-pVTZ Method

Frequency (cm^{-1})	Band Position (μm)	Intensity (km mol^{-1})	Frequency (cm^{-1})	Band Position (μm)	Intensity (km mol^{-1})
234	42.70	3.5	1266	7.901	17.4
267	37.52	19.0	1279	7.817	83.0
336	29.77	8.1	1299	7.697	50.6
399	25.06	0.0	1340	7.464	3.6
420	23.81	0.7	1351	7.403	0.7
425	23.51	1.1	1360	7.352	0.5
465	21.51	3.4	1363	7.337	3.4
510	19.61	0.0	1364	7.332	0.0
525	19.06	4.1	1377	7.260	3.4
529	18.92	2.1	1386	7.217	2.0
593	16.86	1.5	1407	7.107	21.4
684	14.63	20.5	1413	7.076	14.7
696	14.37	20.4	1422	7.031	24.6
715	13.98	48.1	1443	6.930	26.7
799	12.52	63.8	1485	6.733	0.2
832	12.02	23.8	1494	6.694	3.2
846	11.83	19.5	1500	6.666	24.6
857	11.67	7.4	1505	6.646	24.4
901	11.09	51.4	1525	6.558	10.2
939	10.65	2.0	1629	6.138	54.3
962	10.40	0.1	2975	3.361	57.1

Table 4
(Continued)

Frequency (cm^{-1})	Band Position (μm)	Intensity (km mol^{-1})	Frequency (cm^{-1})	Band Position (μm)	Intensity (km mol^{-1})
986	10.15	43.1	3054	3.274	53.4
1041	9.611	116.7	3056	3.273	35.0
1043	9.590	117.3	3062	3.266	70.4
1055	9.475	54.5	3070	3.257	76.4
1064	9.401	4.7	3075	3.252	18.9
1069	9.351	3.2	3103	3.222	5.9
1075	9.303	7.7	3107	3.218	43.7
1076	9.296	20.8	3109	3.216	41.4
1103	9.063	0.6	3148	3.176	0.2
1190	8.407	60.3	3149	3.175	25.6
1221	8.187	0.0	3555	2.813	3.1
1247	8.018	93.5	3646	2.743	7.8

Table 5
Harmonic Vibrational Frequencies (cm^{-1}) and IR Intensities (km mol^{-1}) of HMT-CH$_3$ (C_1 Symmetry) Computed Using the ωB97X-D/cc-pVTZ Method

Frequency (cm^{-1})	Band Position (μm)	Intensity (km mol^{-1})	Frequency (cm^{-1})	Band Position (μm)	Intensity (km mol^{-1})
212	47.22	0.0	1283	7.795	72.7
237	42.21	0.3	1287	7.773	75.3
301	33.21	0.8	1344	7.443	0.3
409	24.48	0.0	1351	7.404	3.7
419	23.88	0.3	1354	7.384	2.2
430	23.27	0.6	1366	7.319	1.4
471	21.25	1.3	1373	7.284	0.2
491	20.36	0.6	1378	7.256	3.5
534	18.72	4.0	1382	7.237	1.4
540	18.51	2.8	1399	7.150	1.8
579	17.27	2.8	1401	7.139	11.9
684	14.63	21.8	1421	7.038	19.2
699	14.29	19.9	1427	7.008	19.8
716	13.97	22.7	1435	6.968	21.9
789	12.67	7.0	1497	6.682	1.6
825	12.13	13.2	1499	6.670	0.1
833	11.99	8.1	1506	6.641	15.5
861	11.62	11.9	1508	6.631	7.7
947	10.56	38.6	1520	6.578	17.9
951	10.52	0.4	1528	6.543	9.3
970	10.31	0.1	1542	6.486	7.0
1002	9.984	18.8	3041	3.288	18.9
1032	9.690	53.6	3054	3.274	44.5
1056	9.466	115.9	3055	3.274	50.5
1064	9.403	28.2	3061	3.267	72.6
1065	9.392	69.6	3067	3.260	74.5
1066	9.382	36.8	3069	3.258	21.8
1076	9.291	6.7	3076	3.251	10.1
1091	9.162	4.5	3104	3.222	0.4
1115	8.971	14.4	3108	3.218	40.4
1150	8.694	13.7	3108	3.218	40.8
1161	8.610	44.9	3120	3.205	21.1
1249	8.008	0.4	3122	3.203	35.8
1262	7.922	53.9	3150	3.175	12.4
			3152	3.172	30.8

Table 6
Harmonic Vibrational Frequencies (cm^{-1}) and IR Intensities (km mol^{-1}) of HMT-CN (C_I Symmetry) Computed Using the ωB97X-D/cc-pVTZ Method

Frequency (cm^{-1})	Band Position (μm)	Intensity (km mol^{-1})	Frequency (cm^{-1})	Band Position (μm)	Intensity (km mol^{-1})
131	76.61	4.4	1234	8.104	0.0
150	66.72	3.6	1279	7.818	63.7
346	28.90	0.8	1288	7.767	73.1
383	26.12	0.5	1338	7.476	0.0
396	25.28	0.0	1341	7.456	6.0
411	24.31	1.4	1354	7.384	3.7
464	21.56	0.3	1355	7.380	0.1
476	21.00	1.7	1361	7.350	0.3
530	18.85	2.7	1370	7.300	0.0
531	18.82	2.1	1381	7.243	6.1
570	17.53	7.3	1396	7.164	34.5
580	17.25	1.6	1397	7.158	9.6
680	14.71	25.9	1401	7.135	6.4
700	14.29	18.6	1427	7.010	13.1
712	14.03	31.3	1495	6.691	2.5
818	12.23	1.6	1501	6.661	9.5
853	11.72	16.9	1513	6.609	18.6
867	11.54	12.7	1514	6.607	19.4
877	11.40	10.8	1535	6.514	5.3
950	10.52	10.0	2404	4.159	0.3
966	10.35	0.0	3060	3.268	25.6
970	10.31	1.1	3061	3.267	24.3
1031	9.701	76.4	3064	3.264	41.4
1049	9.531	106.1	3067	3.261	62.0
1052	9.507	126.7	3071	3.256	46.1
1061	9.423	41.7	3078	3.249	6.9
1064	9.395	23.7	3114	3.212	0.1
1074	9.307	0.9	3117	3.209	25.0
1082	9.238	0.9	3117	3.208	23.6
1101	9.079	53.7	3123	3.202	24.2
1106	9.040	7.8	3125	3.200	24.5
1222	8.186	69.4	…	…	…

Table 7
Harmonic Vibrational Frequencies (cm^{-1}) and IR Intensities (km mol^{-1}) of HMT-OCN (C_I Symmetry) Computed Using the ωB97X-D/cc-pVTZ Method

Frequency (cm^{-1})	Band Position (μm)	Intensity (km mol^{-1})	Frequency (cm^{-1})	Band Position (μm)	Intensity (km mol^{-1})
46	217.2	2.7	1180	8.475	232.1
115	87.17	2.9	1236	8.088	9.0
216	46.31	3.0	1238	8.074	77.0
297	33.63	1.7	1284	7.790	78.5
388	25.77	0.4	1292	7.741	83.4
390	25.65	0.1	1334	7.494	3.5
417	23.98	0.9	1348	7.418	0.6
456	21.95	1.2	1351	7.401	1.7
497	20.11	1.3	1355	7.379	1.2
525	19.06	2.6	1361	7.349	3.1
526	18.99	4.3	1372	7.286	6.7
536	18.65	3.2	1376	7.269	1.2
554	18.05	4.3	1399	7.149	37.6
644	15.52	6.9	1403	7.130	8.7
690	14.49	22.1	1427	7.008	23.5
695	14.39	17.6	1433	6.976	15.5
725	13.79	41.8	1490	6.711	0.9
820	12.19	3.1	1500	6.665	5.9
859	11.64	16.7	1504	6.649	23.2
866	11.54	15.2	1511	6.616	25.6
886	11.29	4.9	1531	6.534	9.4
957	10.45	2.1	2405	4.157	230.0

Table 7
(Continued)

Frequency (cm^{-1})	Band Position (μm)	Intensity (km mol^{-1})	Frequency (cm^{-1})	Band Position (μm)	Intensity (km mol^{-1})
963	10.38	10.8	3060	3.268	42.0
981	10.19	7.0	3065	3.262	24.8
1024	9.764	307.5	3069	3.258	23.3
1040	9.611	83.7	3076	3.251	61.7
1056	9.468	110.5	3080	3.247	46.7
1064	9.396	22.0	3085	3.241	4.9
1069	9.354	7.0	3113	3.212	14.2
1074	9.307	7.2	3121	3.204	18.9
1079	9.272	22.4	3123	3.202	24.7
1085	9.214	11.9	3135	3.190	10.6
1119	8.937	15.0	3138	3.186	17.0

Table 8
Harmonic Vibrational Frequencies (cm^{-1}) and IR Intensities (km mol^{-1}) of HMT-OCH$_3$ (C_I Symmetry) Computed Using the ωB97X-D/cc-pVTZ Method

Frequency (cm^{-1})	Band Position (μm)	Intensity (km mol^{-1})	Frequency (cm^{-1})	Band Position (μm)	Intensity (km mol^{-1})
87	114.6	2.0	1272	7.860	123.3
154	64.87	0.4	1281	7.808	68.2
185	54.08	4.3	1293	7.735	55.8
279	35.88	3.0	1343	7.446	1.3
348	28.70	0.6	1353	7.391	1.1
392	25.49	0.0	1361	7.349	5.5
412	24.30	1.3	1366	7.320	2.9
452	22.13	1.7	1369	7.304	2.8
483	20.72	0.2	1378	7.257	3.9
523	19.13	1.4	1385	7.220	1.5
528	18.94	2.0	1396	7.163	47.9
544	18.37	5.9	1411	7.086	18.1
587	17.04	0.6	1418	7.053	14.4
687	14.57	23.4	1429	6.998	11.2
697	14.35	17.0	1481	6.753	9.6
718	13.92	29.2	1494	6.692	2.5
821	12.19	4.0	1494	6.691	6.6
858	11.66	16.6	1501	6.662	4.0
872	11.47	13.1	1511	6.619	16.9
887	11.27	11.3	1519	6.585	16.4
956	10.46	25.2	1520	6.580	11.8
967	10.34	4.2	1538	6.503	10.5
989	10.11	22.7	2978	3.358	46.0
1038	9.630	180.6	3009	3.323	66.4
1053	9.498	54.5	3052	3.276	50.2
1055	9.479	136.4	3054	3.275	37.0
1065	9.394	16.7	3060	3.268	71.6
1072	9.328	6.5	3067	3.260	60.1
1078	9.273	9.6	3074	3.253	26.1
1082	9.245	9.8	3084	3.242	30.3
1094	9.142	1.4	3102	3.223	4.0
1123	8.904	13.1	3105	3.220	43.7
1184	8.443	26.7	3110	3.216	36.3
1187	8.424	115.4	3129	3.196	15.5
1226	8.158	108.5	3143	3.182	14.9
1248	8.011	14.2	3147	3.177	21.3

Table 9
Harmonic Vibrational Frequencies (cm^{-1}) and IR Intensities (km mol^{-1}) of HMT-CH(OH)CHO (C_1 Symmetry) Computed Using the ωB97X-D/cc-pVTZ Method

Frequency (cm^{-1})	Band Position (μm)	Intensity (km mol^{-1})	Frequency (cm^{-1})	Band Position (μm)	Intensity (km mol^{-1})
34	292.5	1.3	1227	8.148	45.3
78	128.2	0.6	1245	8.031	0.9
144	69.65	1.2	1280	7.812	76.1
196	51.14	1.6	1284	7.787	14.2
289	34.60	2.3	1293	7.732	88.5
346	28.92	13.1	1330	7.517	16.7
356	28.08	7.8	1349	7.414	1.0
405	24.69	0.1	1354	7.388	0.3
430	23.23	16.2	1358	7.364	0.5
444	22.49	1.2	1365	7.327	0.2
463	21.59	65.1	1368	7.312	0.2
491	20.35	0.7	1377	7.261	1.6
517	19.35	2.7	1381	7.240	0.6
539	18.57	5.7	1402	7.130	21.7
545	18.36	5.2	1409	7.096	35.5
548	18.25	1.1	1413	7.076	28.8
689	14.50	25.6	1418	7.053	10.4
699	14.32	17.4	1423	7.025	25.9
706	14.16	23.4	1463	6.834	35.6
792	12.63	17.6	1495	6.690	0.5
820	12.20	1.2	1504	6.651	22.1
849	11.77	23.0	1511	6.619	7.0
858	11.65	10.6	1526	6.555	16.2
875	11.42	3.0	1543	6.482	7.3
884	11.31	27.3	1831	5.461	191.3
961	10.41	1.3	3001	3.332	4.0
969	10.32	7.6	3024	3.307	48.4
990	10.11	30.1	3056	3.272	2.6
1011	9.889	18.6	3058	3.270	57.6
1045	9.570	151.9	3058	3.270	32.0
1056	9.474	105.2	3063	3.264	97.2
1061	9.425	91.4	3067	3.261	47.0
1063	9.407	18.7	3077	3.250	21.5
1073	9.323	6.4	3108	3.217	4.5
1080	9.260	6.3	3110	3.216	13.8
1090	9.172	3.4	3113	3.212	45.2
1112	8.992	18.3	3114	3.211	33.5
1144	8.742	57.4	3124	3.201	34.9
1193	8.380	51.2	3762	2.658	88.4

Table 10
Harmonic Vibrational Frequencies (cm^{-1}) and IR Intensities (km mol^{-1}) of HMT-NHCHO (C_1 Symmetry) Computed Using the ωB97X-D/cc-pVTZ Method

Frequency (cm^{-1})	Band Position (μm)	Intensity (km mol^{-1})	Frequency (cm^{-1})	Band Position (μm)	Intensity (km mol^{-1})
62	162.0	1.1	1253	7.983	51.2
135	74.22	2.1	1279	7.818	237.2
164	60.82	2.6	1282	7.802	53.1
248	40.33	2.7	1288	7.763	69.2
329	30.44	0.4	1343	7.446	0.8
371	26.96	4.5	1354	7.385	11.0
399	25.05	0.1	1356	7.374	4.3
441	22.69	6.8	1364	7.331	1.1
462	21.64	1.4	1366	7.323	0.7
513	19.48	10.8	1379	7.254	14.8
521	19.21	3.5	1380	7.249	18.5
532	18.80	3.1	1385	7.222	4.7
537	18.63	3.6	1410	7.095	36.2
644	15.52	86.6	1415	7.067	21.2
669	14.94	47.2	1418	7.051	13.4
694	14.41	22.2	1438	6.955	44.3
700	14.29	19.3	1488	6.722	30.8
771	12.97	3.2	1493	6.697	11.9
821	12.18	2.8	1505	6.646	27.8
859	11.64	16.4	1509	6.628	2.0
868	11.53	13.6	1517	6.594	33.2
882	11.34	2.8	1535	6.514	13.1
959	10.43	9.8	1822	5.488	542.8
965	10.37	8.8	3013	3.319	27.9
998	10.02	36.8	3018	3.314	40.9
1035	9.659	178.8	3056	3.272	46.8
1052	9.504	95.9	3061	3.267	29.7
1055	9.479	66.5	3066	3.261	69.2
1064	9.396	12.3	3073	3.254	55.3
1073	9.320	16.1	3079	3.248	13.2
1077	9.285	10.0	3108	3.218	12.8
1082	9.239	0.9	3114	3.212	25.1
1086	9.206	0.9	3116	3.209	31.2
1103	9.063	0.6	3128	3.197	15.9
1194	8.373	45.1	3133	3.192	21.0
1236	8.091	39.8	3637	2.750	30.9

Appendix B

The XYZ coordinates of HMT-OH, HMT-NH₂, HMT-CH₃, HMT-CN, HMT-OCN, HMT-OCH₃, HMT-CH(OH)CHO, and HMT-NHCHO are presented in Tables 11–18, respectively.

Table 11
Atomic *XYZ* Coordinates (in Å) of HMT-OH Using ωB97X-D/cc-pVTZ

N	−1.5098706326	0.8060364163	0.1412484606
C	−0.7099403254	1.2684556528	−0.9944229853
N	0.5024352574	0.4661075980	−1.1890491305
H	−1.3120715983	1.2156484508	−1.9016810059
H	−0.4282070224	2.3097102144	−0.8299134375
C	1.2796007340	0.5662363109	0.0381403124
N	0.5451292295	0.0475379337	1.2020512760
O	2.4745741135	−0.1255169403	−0.1385820094
H	1.4641557641	1.6311565469	0.2254700029
C	−0.6712314732	0.8603153632	1.3381798719
H	−1.2416109133	0.4974185606	2.1937658283
H	−0.3889642019	1.8970732878	1.5291178619
C	−1.8671331412	−0.5951132840	−0.1010019840
C	0.0960026083	−0.9306915158	−1.3942739816
N	−0.6908873866	−1.4474187434	−0.2716307621
H	−0.5002978318	−0.9822937032	−2.3057714704
H	0.9848886465	−1.5431979746	−1.5224271390
C	0.1311688683	−1.3392582417	0.9314195994
H	−2.4545867725	−0.9614890987	0.7424431754
H	−2.4814746791	−0.6516022301	−1.0007234685
H	−0.4339925848	−1.7012073028	1.7913492816
H	1.0164217602	−1.9604676990	0.8136747471
H	2.8795255946	−0.2031281898	0.7276224277
Dipole Moment			
	−0.574	0.320	1.363

Table 12
Atomic *XYZ* Coordinates (in Å) of HMT-NH₂ Using ωB97X-D/cc-pVTZ

N	1.4903010688	0.0027850149	−0.8880979889
C	0.6658784247	1.1887353478	−1.1321630064
N	−0.5365839160	1.2164455526	−0.2944642450
H	1.2590282048	2.0809059280	−0.9275564890
H	0.3711183133	1.2067249538	−2.1828993266
C	−1.3017647113	0.0006389034	−0.5989650601
N	−0.5351116564	−1.2151921462	−0.2982926708
N	−2.5280582530	−0.0012293228	0.1576982848
H	−1.4640712256	0.0022830154	−1.6851769339
C	0.6673371030	−1.1833637714	−1.1359170446
H	1.2615259337	−2.0754879943	−0.9341497784
H	0.3725430077	−1.1983891188	−2.1866912684
C	1.8659790469	0.0007682891	0.5291358291
C	−0.1070342494	1.1813571051	1.1118588808
N	0.7020303291	−0.0013238180	1.4131804887
H	0.4817744481	2.0775221449	1.3128123886
H	−0.9866743132	1.1851386203	1.7499459007
C	−0.1055980475	−1.1840232612	1.1081364505
H	2.4717585309	−0.8836554947	0.7336460032
H	2.4707510286	0.8852294367	0.7364696552
H	0.4843033284	−2.0801160148	1.3061828714
H	−0.9851862785	−1.1908890333	1.7462698698
H	−3.0676189369	−0.8239628361	−0.0710895563
H	−3.0685550887	0.8215748631	−0.0686087695
Dipole Moment			
	−0.723	0.001	−0.991

Table 13
Atomic *XYZ* Coordinates (in Å) of HMT-CH₃ Using ωB97X-D/cc-pVTZ

N	−1.5179854993	0.5553656564	−0.6604235493
C	−0.7000861256	−0.1963509947	−1.6149203447
N	0.5157273343	−0.7433382955	−1.0051719459
H	−1.2936432371	−1.0177094125	−2.0194578306
H	−0.4191755396	0.4636382745	−2.4370601787
C	1.2929385909	0.3923324144	−0.4734925703
N	0.5221172069	1.1298570910	0.5447053995
C	2.6749440801	−0.0127238240	0.0053069846
H	1.4344057856	1.0839492836	−1.3079195816
C	−0.6939053692	1.6304550472	−0.1036599731
H	−1.2838683145	2.1859276742	0.6271757800
H	−0.4125376595	2.3148388829	−0.9054468034
C	−1.8759012569	−0.3485110785	0.4352027547
C	0.0982586442	−1.6140623396	0.0983793909
N	−0.6981976526	−0.9048242461	1.1034631147
H	−0.4967383643	−2.4313142033	−0.3122004985
H	0.9736897465	−2.0490828026	0.5775882322
C	0.1045566237	0.2122459366	1.6090152467
H	−2.4747883783	0.1993534857	1.1645213851
H	−2.4792478103	−1.1666078508	0.0384325280
H	−0.4854826991	0.7728060189	2.3355429357
H	0.9798543877	−0.1827094088	2.1217647417
H	3.2253370557	0.8767063199	0.3068502654
H	3.2037998118	−0.5049775039	−0.8088399747
H	2.6569591818	−0.6947216944	0.8531755777
Dipole Moment			
	0.208	0.027	−0.031

Table 14
Atomic *XYZ* Coordinates (in Å) of HMT-CN Using ωB97X-D/cc-pVTZ

N	−1.8049546995	0.5884783865	0.1365616528
C	−1.0736340356	1.1897371518	−0.9777544644
N	0.2690135368	0.6141485229	−1.1432803256
H	−1.6316325827	1.0352586722	−1.9012105343
H	−0.9798412997	2.2637625388	−0.8093190320
C	0.9814471161	0.8387522889	0.1188567368
N	0.3205827140	0.2019280137	1.2625578411
C	2.3801169799	0.3903586802	0.0144534510
H	1.0107224009	1.9155908287	0.3025452545
C	−1.0233738976	0.7898798209	1.3558052195
H	−1.5414061676	0.3305142798	2.1975138828
H	−0.9297213037	1.8593511762	1.5509872295
C	−1.9021052494	−0.8540607941	−0.1083622501
C	0.1187911140	−0.8351059493	−1.3507402329
N	−0.5869332533	−1.4816138929	−0.2451227515
H	−0.4368961718	−0.9901013866	−2.2754287717
H	1.1048247010	−1.2857517161	−1.4621076321
C	0.1686897933	−1.2346175042	0.9822865426
H	−2.4336331992	−1.3200024059	0.7221708908
H	−2.4746922456	−1.0202701370	−1.0215932512
H	−0.3488041040	−1.6931512697	1.8248010748
H	1.1549254324	−1.6908516090	0.8990169421
N	3.4686907959	0.0411084844	−0.0648801854
Dipole Moment			
	−4.205	0.709	0.206

Table 15
Atomic *XYZ* Coordinates (in Å) of HMT-OCN Using ωB97X-D/cc-pVTZ

N	1.9311387354	0.4563541493	−0.8222652711
C	0.7905482942	1.3363767630	−1.0680678756
N	−0.3794098204	0.9566652456	−0.2560142732
H	1.0611406825	2.3624080155	−0.8220895894
H	0.5213720487	1.2951530837	−2.1243129057
C	−0.6874652884	−0.4106369541	−0.6202021441
N	0.3708864490	−1.3441719241	−0.3157307711
O	−1.8566072329	−0.8676907709	0.0936817264
H	−0.9049697412	−0.4502542903	−1.6896302080
C	1.5267819475	−0.9144329621	−1.1254697704
H	2.3552082322	−1.5914172944	−0.9217341877
H	1.2705971638	−0.9919192223	−2.1830139010
C	2.2669500376	0.5273601086	0.6038420570
C	0.0149888240	1.0169136268	1.1630830470
N	1.1430859534	0.1374331099	1.4564388357
H	0.2831692769	2.0478069754	1.3919414797
H	−0.8327493745	0.7403498591	1.7866426443
C	0.7452107646	−1.2236004718	1.1057329663
H	3.1104517288	−0.1343539531	0.8029821879
H	2.5617579206	1.5483108584	0.8486631283
H	1.5723355874	−1.9077249073	1.2928097522
H	−0.0971361283	−1.5263964784	1.7236013072
C	−2.9285589803	−0.1821188875	−0.0902294232
N	−3.9238654601	0.3809649822	−0.2223439822
Dipole Moment			
	5.427	−0.484	−0.310

Table 17
Atomic *XYZ* Coordinates (in Å) of HMT-CH(OH)CHO Using ωB97X-D/cc-pVTZ

N	2.2028281919	0.2341283302	−0.9931468642
C	1.2259646413	1.3195162480	−1.0650467738
N	0.1217252322	1.1420166903	−0.1104045050
H	1.7271433034	2.2650798456	−0.8531999492
H	0.8131399631	1.3665012135	−2.0734555594
C	−0.5210880602	−0.1435470519	−0.4373641093
N	0.4142615893	−1.2622125609	−0.2929860009
C	−1.8402309969	−0.3654857310	0.3200445578
H	−0.8058546730	−0.1036140346	−1.4918782743
C	1.5063093773	−1.0305985001	−1.2442279417
H	2.2216489565	−1.8501280002	−1.1672261412
H	1.0982894905	−1.0212858492	−2.2556701344
C	2.7332392415	0.1942443612	0.3711717431
C	0.7115228015	1.0755031206	1.2347876723
N	1.6804194171	−0.0099336412	1.3693502705
H	1.2067724263	2.0258489024	1.4387839440
H	−0.0736602712	0.9426949801	1.9793016035
C	0.9934912617	−1.2655610483	1.0519653515
H	3.4567241235	−0.6181447318	0.4504092058
H	3.2465335241	1.1338702117	0.5813696585
H	1.7072759018	−2.0872319455	1.1180680161
H	0.2161796064	−1.4457915825	1.7933449178
O	−2.5173895326	−1.4619265373	−0.2059635403
H	−3.3663259710	−1.1224666778	−0.5183624595
C	−2.6997002001	0.8797317627	0.2361652126
H	−1.6457080478	−0.5281218909	1.3884001510
O	−3.7889258141	0.8437869357	−0.2729369853
H	−2.2860215658	1.8052488990	0.6607096551
Dipole Moment			
	2.571	1.336	0.997

Table 16
Atomic *XYZ* Coordinates (in Å) of HMT-OCH$_3$ Using ωB97X-D/cc-pVTZ

N	1.7758125296	0.0440734287	−0.8630321674
C	0.7466449582	0.9613727771	−1.3531832617
N	−0.4399923464	0.9756908919	−0.4922339157
H	1.1605036298	1.9693411984	−1.4007400730
H	0.4541764124	0.6627611089	−2.3614423868
C	−0.9677164896	−0.3980544920	−0.4489633134
N	0.0084054874	−1.3360543191	0.0912948343
O	−2.1123603713	−0.4750354182	0.3284758277
H	−1.1847591135	−0.6906205984	−1.4860016033
C	1.1839594070	−1.2924575440	−0.7840238422
H	1.9287730799	−1.9918090399	−0.4031527651
H	0.8948322675	−1.6128102103	−1.7863582260
C	2.1401380446	0.4555054065	0.4967282155
C	−0.0178936210	1.3650272629	0.8603057764
N	0.9938207798	0.4601183370	1.4056659576
H	0.3907698759	2.3755883858	0.8162443137
H	−0.8867425025	1.3687797900	1.5155147209
C	0.4200861174	−0.8868108023	1.4288628321
H	2.8964309758	−0.2305292390	0.8812540203
H	2.5716476272	1.4571740289	0.4602761690
H	1.1639328210	−1.5875676167	1.8097931075
H	−0.4444220162	−0.9017901862	2.0879145489
H	−3.4971515359	−0.2042132280	−1.1875892328
C	−3.2177392853	0.2114019987	−0.2129004995
H	−4.0425266210	0.0705881211	0.4809959343
H	−3.0113240746	1.2768016206	−0.3323521895
Dipole Moment			
	−0.173	0.792	−0.944

Table 18
Atomic *XYZ* Coordinates (in Å) of HMT-NHCHO Using ωB97X-D/cc-pVTZ

N	2.1080905393	0.4886645018	−0.7041715269
C	1.0992185455	1.5479121743	−0.6656881429
N	−0.1331553551	1.1179910078	0.0095853024
H	1.5067720927	2.4103286499	−0.1385613991
H	0.8589592611	1.8504671435	−1.6858406834
C	−0.6341537544	−0.0342370355	−0.7430229505
N	0.3107609102	−1.1534964761	−0.7348393117
N	−1.9027177350	−0.4898275409	−0.2317076089
H	−0.7303349327	0.2891424049	−1.7852684146
C	1.5355701865	−0.6704901474	−1.3885234979
H	2.2677018849	−1.4779106230	−1.3993200141
H	1.3054764039	−0.4022838550	−2.4205008981
C	2.4055062728	0.0973125167	0.6766002906
C	0.2214304823	0.7054434964	1.3762587879
N	1.2142687489	−0.3676477324	1.3877133845
H	0.6217515049	1.5741501402	1.8989378990
H	−0.6724017137	0.3693680443	1.8978216242
C	0.6524699300	−1.5003827493	0.6552151739
H	3.1488308700	−0.7009531004	0.6673456381
H	2.8261144832	0.9539546809	1.2047155551
H	1.3781242796	−2.3136290234	0.6318537736
H	−0.2390698898	−1.8515868379	1.1713396539
H	−2.1280024350	−1.4555135471	−0.4135034017
C	−2.9480110070	0.3243596941	0.0821634863
O	−4.0653021350	−0.0730667635	0.3093595597
H	−2.6596234512	1.3848714651	0.1319976566
Dipole Moment			
	4.393	0.377	−1.073

ORCID iDs

Partha P. Bera ⓘ https://orcid.org/0000-0003-0843-3209
Scott A. Sandford ⓘ https://orcid.org/0000-0002-6034-9816
Timothy J. Lee ⓘ https://orcid.org/0000-0002-2598-2237
Michel Nuevo ⓘ https://orcid.org/0000-0003-1527-2669

References

Allamandola, L. J., Sandford, S. A., & Valero, G. J. 1988, Icar, 76, 225
Ashbourn, S. F. M., Elsila, J. E., Dworkin, J. P., et al. 2007, M&PS, 42, 2035
Barone, V., Biczysko, M., & Bloino, J. 2014, PCCP, 15, 751
Bennett, C. J., & Kaiser, R. I. 2007, ApJ, 600, 1289
Bera, P. P., Head-Gordon, M., & Lee, T. J. 2013, PCCP, 15, 2012
Bera, P. P., Nuevo, M., Materese, C. K., et al. 2016, JChPh, 144, 144308
Bera, P. P., Nuevo, M., Milam, S., et al. 2010, JChPh, 133, 104303
Bera, P. P., Peverati, R., Head-Gordon, M., & Lee, T. J. 2015, PCCP, 17, 1859
Bera, P. P., Stein, T., Head-Gordon, M., & Lee, T. J. 2017, AsBio, 17, 771
Bernstein, M. P., Dworkin, J. P., Sandford, S. A., et al. 2002a, Natur, 416, 401
Bernstein, M. P., Dworkin, J. P., Sandford, S. A., & Allamandola, L. J. 2001, M&PS, 36, 351
Bernstein, M. P., Elsila, J. E., Dworkin, J. P., et al. 2002b, ApJ, 576, 1115
Bernstein, M. P., Moore, M. H., Elsila, J. E., et al. 2003, ApJL, 582, L25
Bernstein, M. P., Sandford, S. A., Allamandola, L. J., et al. 1995, ApJ, 454, 327
Bernstein, M. P., Sandford, S. A., Allamandola, L. J., et al. 1999, Sci, 283, 1135
Bernstein, M. P., Sandford, S. A., Allamandola, L. J., & Chang, S. 1994, JPhCh, 98, 12206
Boese, A. D., & Martin, J. M. L. 2004, JPCA, 108, 3085
Callahan, M. P., Gerakines, P. A., Martin, M. G., et al. 2013, Icar, 226, 1201
Cané, E., Miani, A., & Trombetti, A. 2007, JPCA, 111, 8218
Cottin, H., Bachir, S., Raulin, F., & Gazeau, M.-C. 2002, AdSpR, 30, 1481
Cottin, H., Szopa, C., & Moore, M. H. 2001, ApJL, 561, L139
de Marcellus, P., Bertrand, M., Nuevo, M., et al. 2011, AsBio, 11, 847
Dunning, T. H. 1989, JChPh, 90, 1007
Dworkin, J. P., Deamer, D. W., Sandford, S. A., & Allamandola, L. J. 2001, PNAS, 98, 815
Dworkin, J. P., Gillette, J. S., Bernstein, M. P., et al. 2004, AdSpR, 33, 67
Fortenberry, R. C., & Lee, T. J. 2019, Annu. Rev. Comp. Chem., in press
Gerakines, P. A., Moore, M. H., & Hudson, R. L. 2001, JGR, 106, 33381
Hulett, H. R., Wolman, Y., Miller, S. L., et al. 1971, Sci, 174, 1038
Huang, X., & Lee, T. J. 2008, JChPh, 129, 044312

Iwakami, Y., Takazono, M., & Tsuchiya, T. 1968, Bull. Chem. Soc. Japan, 41, 813
Johnson, R. D. 2018, Computational Chemistry Comparison and Benchmark DataBase v20, NIST, doi:10.18434/T47C7Z
Lee, T. J., Dateo, C. E., Gazdy, B., & Bowman, J. M. 1993, JPhCh, 97, 8937
Lee, T. J., Martin, J. M. L., Dateo, C. E., & Taylor, P. R. 1995a, JPhCh, 99, 15858
Lee, T. J., Martin, J. M. L., & Taylor, P. R. 1995b, JChPh, 102, 254
Mackie, C. J., Candian, A., Huang, X., et al. 2015, JChPh, 143, 224314
Mackie, C. J., Candian, A., Huang, X., et al. 2018, PCCP, 20, 1189
Mardirossian, N., & Head-Gordon, M. 2017, MolPh, 115, 2315
Martin, J. M. L., Lee, T. J., & Taylor, P. R. 1992, JChPh, 97, 8361
Martin, J. M. L., Lee, T. J., & Taylor, P. R. 1993, JMoSp, 160, 105
Materese, C. K., Nuevo, M., Bera, P. P., et al. 2013, AsBio, 13, 948
Materese, C. K., Nuevo, M., McDowell, B. L., et al. 2018, ApJ, 864, 44
Materese, C. K., Nuevo, M., & Sandford, S. A. 2017, AsBio, 17, 761
Materese, C. K., Nuevo, M., Sandford, S. A., et al. 2019, AsBio, submitted
Meierhenrich, U. J., Muñoz Caro, G. M., Schutte, W. A., et al. 2005, Chemistry, 11, 4895
Meinert, C., Myrgorodska, I., de Marcellus, P., et al. 2016, Sci, 352, 208
Minenkov, Y., Singstad, Å., Occhipinti, G., & Jensen, V. R. 2012, Dalton Trans., 41, 5526
Moore, M. H., & Hudson, R. L. 1998, Icar, 135, 518
Muñoz Caro, G. M., Meierhenrich, U., Schutte, W. A., et al. 2004, A&A, 413, 209
Muñoz Caro, G. M., Meierhenrich, U. J., Schutte, W. A., et al. 2002, Natur, 416, 403
Muñoz Caro, G. M., & Schutte, W. A. 2003, A&A, 412, 121
Nuevo, M., Auger, G., Blanot, D., & d'Hendecourt, L. 2008, OLEB, 38, 37
Nuevo, M., Bredehöft, J. H., Meierhenrich, U. J., et al. 2010, AsBio, 10, 245
Nuevo, M., Chen, Y.-J., Yih, T.-S., et al. 2007, AdSpR, 40, 1628
Nuevo, M., Cooper, G., & Sandford, S. A. 2018, NatCo, 9, 5276
Nuevo, M., Materese, C. K., & Sandford, S. A. 2014, ApJ, 793, 125
Nuevo, M., Milam, S. N., Sandford, S. A., et al. 2009, AsBio, 9, 683
Nuevo, M., Milam, S. N., & Sandford, S. A. 2012, AsBio, 12, 295
Nuevo, M., Sandford, S. A., Materese, C. K., & Cooper, G. W. 2015, American Chemical Society Fall Meeting Abstracts, 272
Sandford, S. A., Bera, P. P., Lee, T. J., et al. 2015, in Photoinduced Phenomena in Nucleic Acids II, ed. M. Barbatti, A. C. Borin, & S. Ullrich (Berlin: Springer), 123, doi:10.1007/128_2013_499
Sephton, M. A. 2002, Nat. Prod. Rep., 19, 292
Shao, Y., Gan, Z., Epifanovsky, E., et al. 2015, MolPh, 113, 184
Shock, E. L., & Schulte, M. D. 1990, GeCoA, 54, 3159
Vinogradoff, V., Bernard, S., Le Guillou, C., & Remusat, L. 2018, Icar, 305, 358
Wang, Y., Zhang, Y., Ni, H., et al. 2015, AcSpA, 135, 296